International Journal of Biological Macromolecules 204 (2022) 593–605

Contents lists available at ScienceDirect

International Journal of Biological Macromolecules

journal homepage: www.elsevier.com/locate/ijbiomac

Uniform rod and spherical nanocrystalline celluloses from hydrolysis of industrial pepper waste (*Piper nigrum* L.) using organic acid and inorganic acid

Holilah Holilah [a,c], Hasliza Bahruji [b], Ratna Ediati [a], Asranudin Asranudin [a,c], Aishah Abdul Jalil [d,e], Bambang Piluharto [f], Reva Edra Nugraha [g], Didik Prasetyoko [a,*]

[a] Department of Chemistry, Faculty of Science and Data Analytics, Institut Teknologi Sepuluh Nopember, Sukolilo, Surabaya, 60111, Indonesia
[b] Centre of Advanced Material and Energy Sciences, Universiti Brunei Darussalam, Jl. Tungku Link, BE 1410, Brunei
[c] Department of Food Science and Technology, Faculty of Agriculture, Halu Oleo University, Kendari, Indonesia
[d] Department of Chemical Engineering, Faculty of Chemical and Energy Engineering, Universiti Teknologi Malaysia, 81310 UTM, Skudai, Johor Bahru, Johor, Malaysia
[e] Centre of Hydrogen Energy, Institute of Future Energy, Universiti Teknologi Malaysia, 81310, UTM, Skudai, Johor Bahru, Johor, Malaysia
[f] Department of Chemistry, Faculty of Mathematics and Natural Sciences, University of Jember, Indonesia
[g] Department of Chemical Engineering, Faculty of Engineering, Universitas Pembangunan Nasional "Veteran" Jawa Timur, Surabaya 60294, Indonesia

ARTICLE INFO

Keywords:
Pepper waste
Hydrolysis
Inorganic acid
Organic acid
Sonication
Nanocellulose

ABSTRACT

Conversion of lignocellulosic biowastes from agricultural industry into nanocrystalline cellulose provides pathway to reduce environmental pollution while enhancing the economic value of biowastes. Nanocellulose (NCC) with uniform morphology was isolated from pepper (*Piper nigrum L.)* stalk waste (PW) using acid hydrolysis method. The role of inorganic acids (sulfuric acid, hydrochloric acid, phosphoric acid), organic acids (oxalic acid, citric acid, acetic acid) and variation of sonication times were investigated on the physicochemical characteristics, self-assembled structure, crystallinity, particle size, zeta potential and thermal stability of the isolated nanocellulose. Hydrolysis using inorganic acids transformed cellulose from PW into a spherical shaped NCC at ~33–67 nm of average diameter. Meanwhile hydrolysis in organic acids produced rod-shaped NCC at 210–321 nm in length. This study highlighted the role of acidity strength for organic acid and inorganic acid in controlling the level of hydrogen bond dissociation and the dissolution of amorphous fragments, which consequently directing the morphology and the physicochemical properties of NCCs.

1. Introduction

Indonesia is the world's largest white pepper producer, generating ~90,000 tons of pepper in 2019 (Direktorat Jenderal Perkebunan Indonesia report). The industrial processing of pepper discarded ~80% of waste in the form of fruit peel and stalk. Most of the discarded waste is decomposed via open burning which caused serious harm to the environment. Pepper waste is suitable for conversion into nanocellulose due to the high level of cellulose content determined at approximately 77.9% [1]. Nanocrystalline cellulose (NCC) is an increasingly important biomaterial for a variety of industrial applications such as biomedical implant [2], food additives [3] and reinforcement agents for polymer composites ([4,5]; Sabarudiin et al., 2020; Omran et al., 2021). NCC is a lightweight material with high thermal and mechanical stabilities, ideal as reinforcement agent in biopolymer composite [6]. The properties of nanocellulose derived from biomass such as morphology, crystallinity and size are greatly influenced by the isolation method and the source of biomass wastes. Lignocellulosic biomass is available in abundance and classified as renewable and biodegradable material for nanocellulose production [7,8]. Biomass waste such as sugarcane bagasse [9], corn husk [10], straw pulp [11], pineapple leaf fiber [12], rice husk [13,14], and oil palm empty fruit bunch [15] have been investigated for production of nanocellulose.

Most of the nanocellulose from biomass waste is obtained using acid hydrolysis process. Inorganic acid such as HCl, H_2SO_4, H_3PO_4 and a mixture of two different acids have been utilized for hydrolysis of cellulose [16] [17]. Recently, natural organic acid was used to replace inorganic acid as potential green catalyst in hydrolysis. Citric acid,

* Corresponding author.
E-mail address: didikp@chem.its.ac.id (D. Prasetyoko).

https://doi.org/10.1016/j.ijbiomac.2022.02.045
Received 12 September 2021; Received in revised form 14 January 2022; Accepted 9 February 2022
Available online 12 February 2022

Fig. 1. Images of (a) pepper tree, (b) dried pepper stalk fibers, (c) pepper stalk powder after milling and (d) PW Cellulose.

oxalic acid and formic acid produced high crystalline cellulose (Nagarajan, Balaji, Kasi Rajan, & Ramanujam, 2020) [13,18–23]. Apart from that, NCC produced from hydrolysis using organic acid has relatively a higher thermal stability compared to sulfuric acid [24]. Nonetheless, hydrolysis is a random process resulted in the formation of nanocellulose with various structure and morphology. Hydrolysis using inorganic acid produced rod-like NCC (Chen, Hasanulbasori, Chiat, & Lee, 2019), cellulose nanowhisker [25] and spherical shaped nanocellulose [26]. Meanwhile organic acids preserved most of the crystal structure and the thermal stability of nanocellulose (Nagarajan, Balaji, Kasi Rajan, & Ramanujam, 2020b).

This study is a continuation of our previously reported work on the conversion of pepper stalk waste into microcrystalline cellulose [1]. Conversion of cellulose extracted from industrial pepper into highly crystalline nanocellulose will be investigated in order to increase the value-added properties of the agriculture waste. This research aimed to establish the effect of different types of acids in controlling the morphology and the properties of nanocellulose. To our knowledge, there is no detail investigation to correlate the types of acids used in hydrolysis with morphology, thermal stability, and physicochemical properties of nanocellulose. Therefore, the effect of various acid solutions categorized as organic acid and inorganic acid will be investigated, in which the results highlighted the potential of organic acid to form rod shape crystalline cellulose meanwhile inorganic acid produced spherical shape nanocrystalline cellulose. The degree of acid dissociation potential will be discussed on the ability to dissociate hydrogen bond and to disintegrate amorphous fragment.

2. Material and methods

2.1. Materials

Pepper stalk waste (PW) was obtained from CV. Hanum Shafira, Southeast Sulawesi, Indonesia. The separation of the peppercorn from the fruit stalk was carried out by soaking the harvested pepper in water for seven days. Sodium hydroxide (NaOH, ≥99%), Sulfuric acid (H_2SO_4, 98%), phosphoric acid (H_3PO_4, 85%), and hydrochloric acid (HCl, 37%) were purchased from Merck, Germany. Hydrogen peroxide (H_2O_2, 30% (*w*/w) in H_2O), citric acid monohydrate ($C_6H_8O_7$, ≥99.5%), oxalic acid dihydrate ($C_2H_2O_4$, ≥99%) and acetic acid (CH_3CO_2H, ≥99%) were purchased from Sigma, Singapore.

2.2. Isolation of nanocellulose

Isolation of cellulose from pepper stalk began by immersion of 500 g of the stalk in deionized water at 80 °C for 4 h. After drying at 100 °C, the stalk was milled to form powder. The composition of cellulose, hemicellulose and lignin in pepper waste were previously determined at 7.9 ± 0.8%, 12.1 ± 0.89% and 2.1 ± 0.5% [1]. The resulting powder was mixed with 5% NaOH solution at 1:20 of weight to volume ratios. The mixture was filtered and washed with deionized water until the pH was neutral. The powder was bleached using a mixture of 3% (*v*/v) H_2O_2 and 5% NaOH solution at the powder to reagent ratio of 1:40 (*w*/*v*). The mixture was stirred at 55 °C for 90 min, then separated using vacuum filtration. The resulting powder was washed with deionized water until the pH of supernatant was neutral. The final step was re-alkalization with hydrothermal-assisted method. The re-alkalization process was carried out with the same method as alkalization only replacing the

conventional thermal process into hydrothermal. After the hydrothermal process, the resulting solid was filtered, washed, and dried at 60 °C. The resulting solid is referred as PW cellulose (PW-C). Fig. 1 showed the images of pepper stalk and products from the treatments described in this section.

The cellulose (PW-C) was subsequently hydrolyzed using 5.5 M acid solution at 100 °C for 3 h. The ratio of PW-C to acid was kept at 1:50 (*w/v*). The cellulose suspension was cooled down and continued with ultrasonication using Ultrasonic probe model (Ultrasonic Processor Model FS/000200/T 200 W with anti-noise cabinet, Cheimika, Italia). Ultrasonication was carried out at 5 min interval for 25 min at room temperature with 200 W sonication power. The acids used for hydrolysis were classified into inorganic acid and organic acid. Sulfuric acid (HCl), phosphoric acid (H_3PO_4) and hydrochloric acid (HCl) were used as inorganic acid, meanwhile citric acid (CA), oxalic acid (OA), and acetic acid (AA) were used as organic acid. The concentration of acid was 5.5 M and the resulting nanocrystalline cellulose were labeled as NC-SA, NC-PA, NC-HA, NC-CA, NC-OA, NC-AA, respectively. The variation of sonication time at 0, 5, 10, 15, 20 and 25 min were coded as 0, 1, 2, 3, 4 and 5, respectively. After hydrolysis process, the nanocellulose suspension was washed using deionized water by centrifugation at the gravitational force of 7445 ×*g* for 10 min until the pH remained unchanged at ~6.5–7.0.

2.3. Characterization

2.3.1. Physicochemical properties of NCC

Density, moisture content, pH, water holding capacity, oil holding capacity and swelling index were determined in order to evaluate the physicochemical properties of NCC. The density of NCC was measured via liquid displacement method [27]. 0.5 g of sample was placed in pycnometer and the weight of pycnometer was measured together with the cellulose sample. Xylene was added in pycnometer containing the cellulose. The volume of the sample was calculated from subtracting the volume of xylene in the pycnometer with the volume of xylene that has been added to the sample. The density was determined in triplicates using this following equation.

$$Density\left(\frac{g}{cm^3}\right) = \frac{The\ mass\ of\ sample}{The\ volume\ of\ sample} \quad (1)$$

The moisture content of NCC was measured from the reduction of NCC mass before (W_0) and after dried (W_1) in oven [28]. One gram of NCC was dried in oven at 100 °C. The moisture content of NCC was calculated using the following equation:

$$Moisture\ content = \frac{W_o - W_1}{W_o} \times 100 \quad (2)$$

The acidity of NCC was measured using pH meter. 0.5 g of NCC was dispersed in distilled water and sonicated for 15 min. The pH of the solution was measured using benchtop pH meter, Mettler Toledo, UK.

Water and oil holding capacities (W/OHC) were measured using method reported by Traynham et al. [29]. 1 g of NCC was weighed and added into 10 mL of distilled water. The solution was then shaken for 10 min. After 10 min, the solution was centrifuged (IEC CL40R Refrigerated Centrifuge, Thermo, Germany) at 2482 ×g for 30 min at room temperature. The supernatant was removed, and the hydrated NCC was collected and weighed. The procedures were repeated using soybean oil to determine the OHC (soybean oil density: 0.917 g/mL). Water/oil holding capacity was calculated using the equation shown below:

$$W\Big/OHC\left(\frac{g}{g}\right) = \frac{W_{the\ swelling\ sample} - W_{the\ initial\ sample}}{W_{the\ initial\ sample}} \quad (3)$$

The swelling index was determined based on the method reported by [30]. 1 g of NCC was dispersed in 10 mL of distilled water. The mixture was stirred for 20 min, and the initial volume and final sedimentation after 24 h was measured using measuring cylinder. The swelling index was calculated using the formula below:

$$Swelling\ index = \frac{Initial\ volume\ of\ sample}{Volume\ of\ sample\ after\ dispersing\ in\ water} \quad (4)$$

2.3.2. Fourier transform infrared spectroscopy (FTIR)

The FTIR spectra of PW, PW-C and NCC from PW were recorded using Fourier transform infrared spectroscopy (FTIR 8400S Spectrometer, Shimadzu, Japan). The characterization was carried out to identify the functional groups of NCC. 1 mg of NCC were mixed with 99 mg of KBr followed by pressing the mixture into pellets. The FTIR spectra analysis was recorded in a range of 400–4000 cm^{-1}.

2.3.3. X-ray diffraction (XRD) analysis

The crystallinity phase of PW, PW-C and NCC were evaluated using X-Ray X'Pert Diffractometer Type PW 3040 Powder Diffractometer, Philips, Netherlands. The powder samples were placed on diffraction cells and scanned using Cu Kα radiation, λ = 1.54056 Å, at 40 kV and 30 mA and 2θ range angle from 5 to 50° with a scan speed of 0.0170°/second. The crystallinity index (CI) of the sample was calculated using Segal's empirical method [31] as below:

$$CI(\%) = [(I_{002} - I_{am})/I_{002}] \times 100 \quad (5)$$

where, I_{002}: The maximum intensity of diffraction of the 002 lattice peak (2θ = 22–23°) and I_{am}: The diffraction intensity of amorphous region (2θ = 18–19°).

2.3.4. Scanning Electron Microscopy (SEM) and Energy Dispersive X-Ray Spectroscopy (EDS)

The morphology of cellulose from PW (PW-C) was observed using SEM (Scanning Electron Microscope FlexSEM 1000, Hitachi, Japan) at 10–15 kV. The dried sample was placed on the double-sided carbon tape. Afterwards, Hummer Sputter Coater (Techincs EMS, Inc., VA) was used to coat the sample with Au at 10 mA for 150 s. Meanwhile the elemental components of nanocrystalline cellulose were measured by the energy-dispersive X-ray spectroscopy (EDS).

2.3.5. Particle size and zeta potential analysis

Particle size distribution and zeta potential of NCC were determined out using Nano size Particle Analyzer (Malvern 3000 Zetasizer NanoZS, Malvern Instrument, U.K). The NCC sample was suspended in distilled water and inserted in the cuvette. The samples were analyzed with a particle size analyzer using dynamic light scattering. The measurements were carried out in the range of 0.1–10,000 nm at room temperature and in triplicates. Delsa Nano Software was used to process the data.

2.3.6. Transmission Electron Microscopy (TEM)

The structure, morphology, and size of NCC isolated from PW were analyzed using Transmission Electron Microscopy (HT7700 120 kV Automated TEM, Hitachi, Japan). 1% of NCC was dispersed in distilled water and dripped onto the surface of copper grid. The solvent was dried at room temperature and analyzed. The width and length of the NCC was measured using Image-J software.

2.3.7. Thermal analysis

Thermal stability of NCC was measured using Simultaneous Thermogravimetric Analyzer STA7200, Hitachi, Japan. The samples were placed in alumina crucible and the decomposition thermal was carried out from 28 °C to 600 °C under air atmosphere with the heating rate of 10 °C/min.

2.4. Statistical analysis

All the data were analyzed using ANOVA in which the significance was accepted at $P \leq 0.05$. Data are expressed as means ± standard deviation and the results were taken from independent experiments

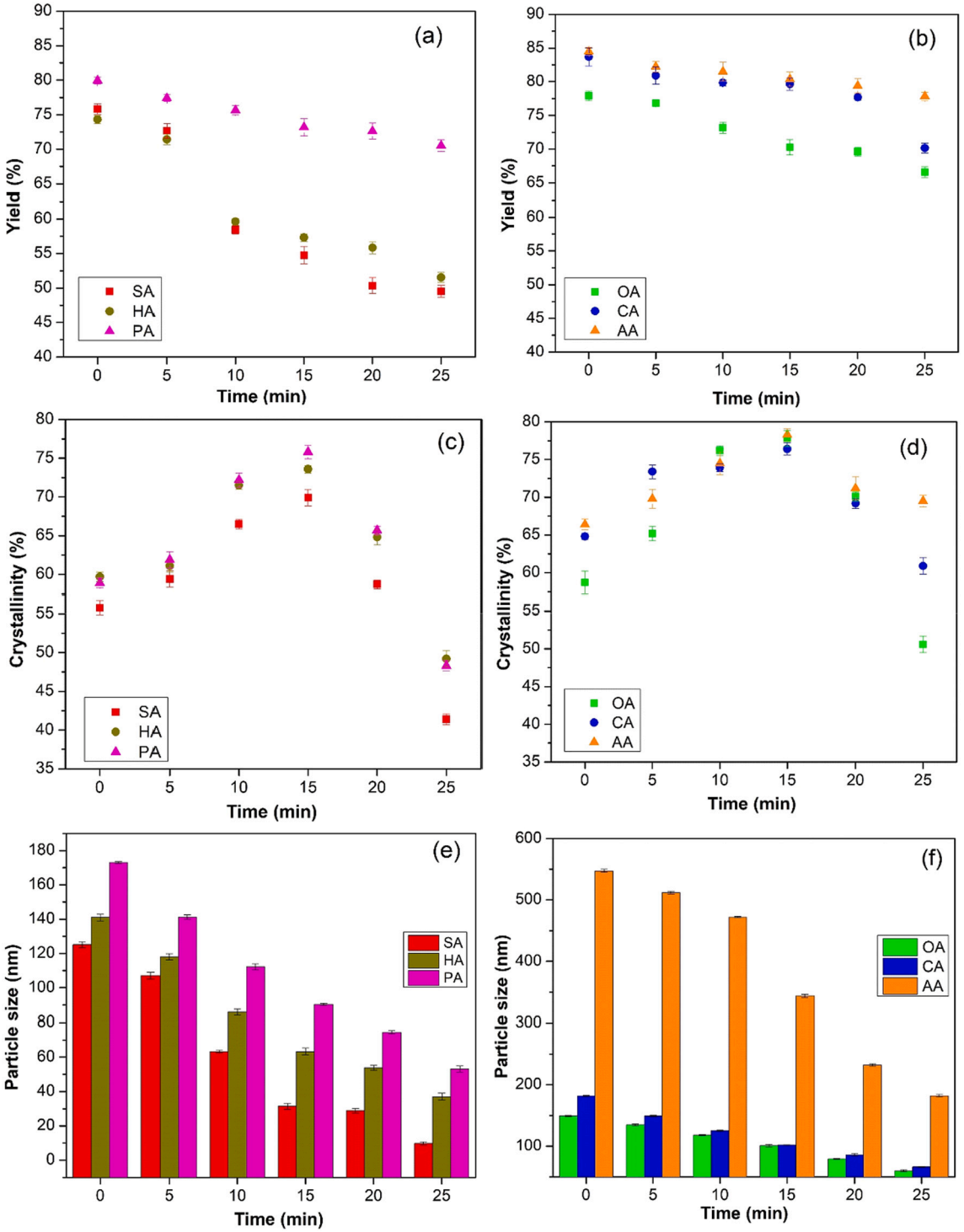

Fig. 2. Effect of sonication time on yield (a,b), crystallinity (c,d) and overall particle size of NCC determined using light scattering particle analyzer (e,f). The nanocelluloses were hydrolyzed using inorganic acids (Sulfuric acid (SA), phosphoric acid (PA) and hydrochloric acid (HA)) and organic acids (citric acid (CA), oxalic acid (OA), and acetic acid (AA)).

performed at least in triplicate measurements.

3. Results and discussion

3.1. Hydrolysis of cellulose PW into NCC

Fig. 2 summarized the yield, the crystallinity, and the particle size of NCC after acid hydrolysis at variation of sonication times. Note that data at 0 min were obtained from acid hydrolysis prior to the sonication. Increasing the sonication time reduced the amount of NCC yields for all different types of acids. However, hydrolysis using inorganic acids (HCl, H_2SO_4 and H_3PO_4) produced relatively a lower NCC yield at ~49.5–79.9% compared to hydrolysis using organic acids (acetic acid, oxalic acid, and citric acid) at 69.6–84.5% (Fig. 2a-b). The highest NCC yield was obtained when hydrolysis was carried using acetic acid at ~80% production (NC-AA). On the other hand, the yield was

Table 1
Physicochemical properties of NCC from pepper waste.

NC	Density (g/cm^3)	Moisture content (%)	pH	Water holding capacity (g/g)	Oil holding capacity (g/g)	Swelling index
NC-SA	1.75 ± 0.05	2.42 ± 0.02	6.43 ± 0.02	12.91 ± 0.06	11.72 ± 0.07	5.45 ± 0.07
NC-HA	1.69 ± 0.03	2.56 ± 0.03	6.34 ± 0.02	11.85 ± 0.08	11.05 ± 0.07	5.15 ± 0.08
NC-PA	1.65 ± 0.05	2.45 ± 0.01	6.50 ± 0.01	11.32 ± 0.05	11.12 ± 0.08	4.95 ± 0.06
NC-OA	1.64 ± 0.05	2.38 ± 0.02	6.55 ± 0.03	11.41 ± 0.07	10.94 ± 0.05	4.72 ± 0.05
NC-CA	1.60 ± 0.03	2.36 ± 0.03	6.35 ± 0.01	10.93 ± 0.08	10.52 ± 0.07	4.75 ± 0.07
NC-AA	1.43 ± 0.04	2.58 ± 0.02	6.54 ± 0.02	7.90 ± 0.05	8.10 ± 0.06	2.95 ± 0.05

significantly lower in sulfuric acid to give 49.5% of NCC after 25 min of hydrolysis (NC-SA).

Optimum crystallinity was obtained at 15 min, however prolonged sonication significantly reduced the crystallinity of NCC (Fig. 2c-d). The degree of crystallinity is associated with the presence of hydrogen bonds that strengthen the interaction between cellulose fragments. Hydrolysis initiated the disintegration of polymeric cellulose network via the dissociation of hydrogen bond. This consequently opened the rigid structure of crystalline cellulose for further hydrolysis and disintegration of amorphous fragment within the crystalline network ([32,33]; Mohd Ishak, Khalil, Abdullah, & Muhd Julkapli, 2020). The crystallinity of NCC was improved within the first 15 min of sonication regardless of the types of acids. However, further sonication up to 25 min reduced the crystallinity due to the hydrolysis not only removed the amorphous fragments, but also destroyed the crystalline structures. The effect of sonication time also revealed a continuous reduction of particle size with prolonged hydrolysis (Fig. 2e-f).

Ultra-sonication treatment formed cavitation which separated the molecules in the amorphous and the crystalline regions. The separation caused the breakdown of the regular parts of the cellulose molecule, resulting in the dissociation of hydrogen bonds and reduction of crystallinity [34]. Therefore, the damage caused by sonication was more pronounced when the sonication was extended beyond the optimum period thus reducing the crystallinity of the cellulose [35,36]. Based on the results, it can be concluded that the optimum sonication time for isolation of nanocellulose from PW-C was measured at 15 min, with no significant differences between the types of acids used in hydrolysis. Therefore, the NCCs obtained after 15 min were used for further characterization.

3.2. Characterization

3.2.1. Physicochemical properties of NCC

NCCs obtained after 15 min were characterized to determine density, moisture content, pH, water holding capacity, oil holding capacity and swelling index (Table 1). Moisture content determines the quality of NCC that affected its application as filler or stabilizing agent. In general, low moisture content indicates a high quality nanocellulose. NCC obtained using organic acids and inorganic acids showed a low moisture content within 2.3–2.5%. The values were approximately similar with the NCC derived from pineapple leaf waste at ~2.34 ± 0.31% [37]. The density of NCCs was determined within 1.43 to 1.75 g/cm^3. NCC produced from hydrolysis using sulfuric acid showed a higher density at 1.75 ± 0.05 g/cm^3 in comparison to the rest of the NCCs. Apart from density, the particle size of NCC obtained from sulfuric acid (NC-SA) was also relatively smaller when compared to the other nanocelluloses. The density of NCCs obtained from PW were comparable with the reported values at 1.5–1.6 g/cm [37,38]. The pH of nanocellulose is used to express the level of acidity or alkalinity of cellulose when dispersed in a solution. The pH of the NCCs were determined within 6.3 to 6.5 which were slightly acidic presumably due to the presence of residual acid that was incorporated within the structure of cellulose. The slight acidic pH was consistent with the studies reported previously by other researchers on nanocellulose produced using acid hydrolysis [39,40].

Water and oil holding capacities represented the ability of NCC to absorb and to hold water/oil within its structure. In general, the transformation of cellulose to NCC enhanced the WHC and OHC, due to the increase of the specific surface area of NCC. Furthermore, reducing the size of cellulose, together with the formation of uniform morphology can contribute to a better oil or water holding capacity. NCC obtained from hydrolysis using sulfuric acid showed the highest WHC and OHC values, at ~12.91 ± 0.06 g/g and 11.72 ± 0.07 g/g, respectively. Swelling index is a parameter to determine the expansion of NCC when submerged in water. The swelling index value has a positive correlation with the WHC/WHO values. NCC with smaller size showed a higher swelling index due to the ability of the nanocellulose to hold water. The lowest swelling index was determined on NCC isolated from acetic acid (NC-AA) at 2.95 ± 0.5.

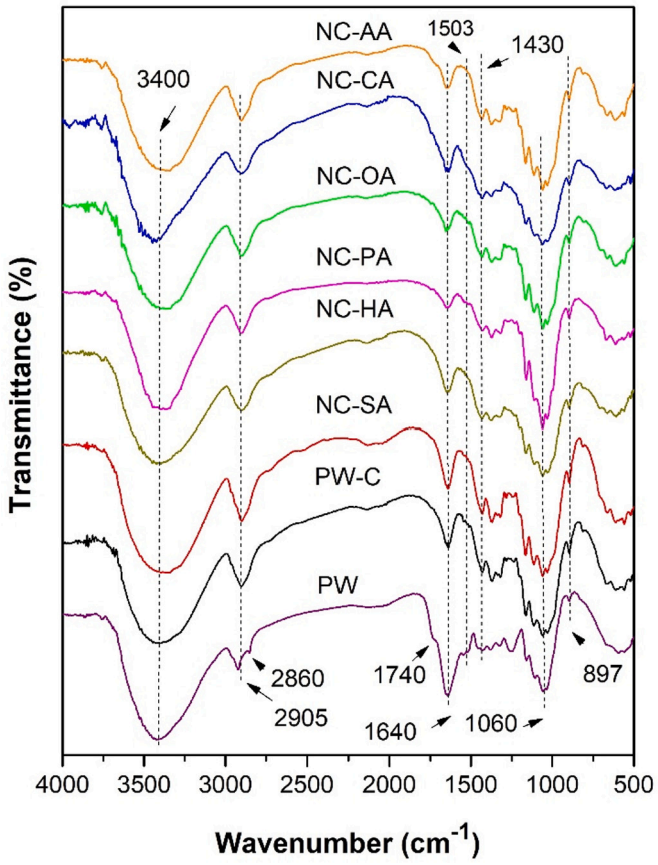

Fig. 3. FT-IR spectra of pepper waste (PW), cellulose from pepper waste (PW-C) and nanocrystalline cellulose hydrolyzed using inorganic acids; sulfuric acid (NC-SA), phosphoric acid (NC-PA) and hydrochloric acid (NC-HA); and organic acids (oxalic acid (NC-OA), citric acid (NC-CA), and acetic acid (NC-AA).

3.2.2. FTIR analysis of NCC

FTIR was used to analyze the functionality of NCC obtained using different types of acids in hydrolysis. The lignocellulose pepper waste (PW) showed the absorption band at 2860 cm^{-1} corresponded to the

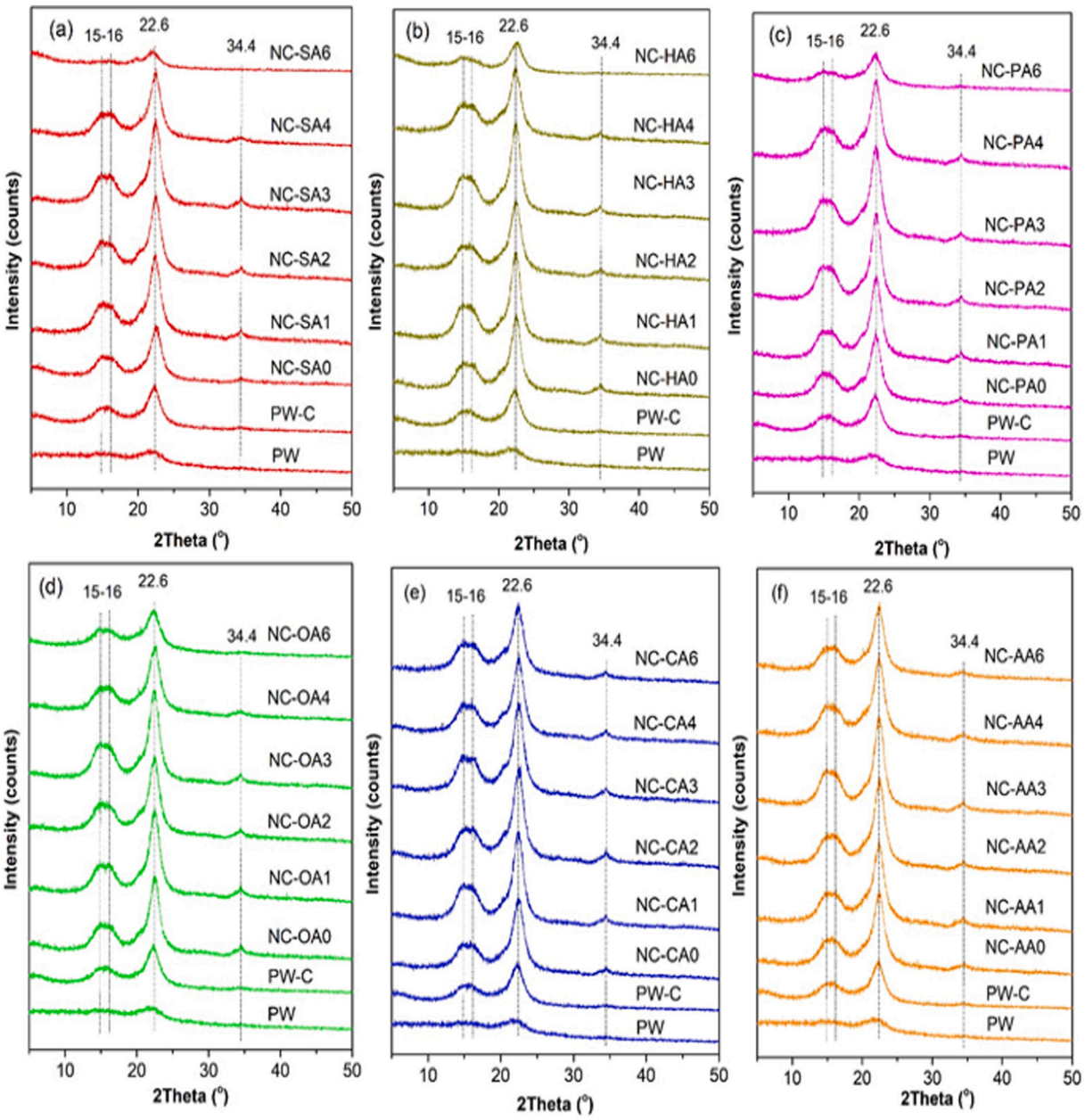

Fig. 4. XRD pattern of PW nanocellulose hydrolyzed by sulfuric acid (a), hydrochloric acid (b), phosphoric acid (c), oxalic acid (d), citric acid (e) and acetic acid (f).

asymmetric and symmetric stretching vibrations of the CH_2 groups of hemicellulose. The PW also showed the absorption band of C═O at 1740 cm^{-1} which was associated with the presence of ketone, aldehyde, or carboxylic acid groups in hemicellulose [41]. In addition, the band at 1503 cm^{-1} was assigned to C═C aromatic skeletal vibration of ester linkage of lignin. Following transformation of pepper waste into cellulose (PW-C) via alkalization and bleaching processes, the lignin and hemicellulose contents were significantly reduced, evidenced from the disappearance of the peaks at 1509 cm^{-1} and 1740 cm^{-1} respectively [1]. All the NCCs hydrolyzed using various types of acids showed similar absorption bands at 897, 1060, 1430, 1640, 2905, 3400 cm^{-1} (Fig. 3) as the cellulose derived from pepper waste, PW-C.

The absorption band at 3400 cm^{-1} was assigned to the O—H group stretching vibration, which represented the hydrophilicity of the samples [42]. The peak was accompanied with the OH bending band at ~1645 cm^{-1} [16]. The adsorption band appeared at 2901 cm^{-1} was corresponded to the aliphatic saturated C—H stretching vibration [43–45]. The C-O-C stretching of the β-1,4-glycosidic linkages in PW-C and C—H rocking vibration were observed at 1060 cm^{-1} and 897 cm^{-1}, respectively [45–47]. The absorption band at 1430 cm^{-1} was assigned to the bending vibration of symmetric CH_2 and the band was also referred as the crystallinity band of the cellulose [25,48].

3.2.3. X-ray diffraction

Fig. 4 showed the XRD analysis of PW, PW-C and NCCs obtained from hydrolysis using inorganic acids and organic acids at different sonication times. PW showed a broad hump centered at 22.6° which is a typical characteristic of amorphous lignocellulose. Cellulose (PW-C) showed the formation of two broad peaks at 15-16° and 22.9° indicating the formation of crystalline cellulose following removal of lignin and hemicellulose fragments. Following hydrolysis with acids (0 sonication time), the main characteristic peaks of crystalline cellulose appeared at 2θ = 15.0°; 16.4°; 22.9° and 34.3° corresponded to (110), (110), (200), and (004) lattice crystallographic planes of cellulose type I, respectively [5,49]. NCC exhibited a higher crystallinity than PW-C due to further removal of amorphous cellulosic fragments during acid hydrolysis [50].

Table 2
Properties of nanocellulose isolated form pepper waste hydrolyzed using various acids.

Sample[a]	Crystallinity Index (%)	Yield (%)[b]	Zeta Potential (mV)	Particle size (nm)			Shape
				PSA[c]	TEM[d]		
					Diameter	Length	
PW	48.3	–	–	–	–	–	Rod like structure
PW-C	51.6	–	–	–	–	–	Rod like structure
NC-SA	69.9	58.4	−37.9 ± 2.4	31.34 ± 1.7	33.4 ± 11.7	–	Spherical
NC-HA	73.7	59.6	−33.2 ± 0.3	63.33 ± 1.9	50.7 ± 9.6	–	Spherical
NC-PA	75.8	75.6	−28.9 ± 2.1	90.30 ± 0.6	67.8 ± 3.1	–	Spherical
NC-OA	77.8	73.2	−28.0 ± 1.9	100.7 ± 2.0	21.7 ± 4.9	210.9 ± 53.1	Rod like structure
NC-CA	76.4	79.7	−28.3 ± 0.9	102.0 ± 0.5	23.2 ± 0.6	258.8 ± 58.4	Rod like structure
NC-AA	78.3	80.3	−23.4 ± 0.6	343.7 ± 2.3	48.7 ± 9.4	321.5 ± 47.2	Rod like structure

[a] The nanocellulose samples (NC) are referred to NCC obtained at 15 of sonication time (NC3).
[b] Yields of nanocelluloses were calculated based on the weight of solid after 15 sonication time.
[c] Determined using particle size analyzer with DLS method.
[d] The average diameter and length were determined from the TEM analysis using ImageJ analysis software.

Increasing the sonication time to 15 min enhanced the peak intensity regardless of the types of acids used. The dissociated H^+ diffused into the framework of cellulose and dissolved the amorphous cellulosic fragments [51]. However, there is a possibility that the disintegrated amorphous fragment is trapped within the interconnected crystalline layer. Therefore, subsequent sonication facilitated the removal of amorphous fragments [32,33]. Apart from removal of the amorphous fragment, hydrolysis also disintegrated the larger crystallites into monocrystals cellulose, particularly when the hydrolysis was carried out using a strong acid. There is also a possibility that crystallinity was increased due to rearrangement of the monocrystal structure through the formation of inter and intramolecular hydrogen bonds [52]. The free movement of the monocrystal cellulose is limited by the formation of hydrogen bond via regular and parallel chains [22]. As summarized in Table 2, NCC from sulfuric acid has low crystallinity index and small particle size compared to the rest of the NCCs.

3.2.4. Particle size and zeta potential analysis

Particle size and zeta potential analysis determined the size and the stability of suspended NCs when dispersed in water (Table 2). In general, the particles size of NCCs were relatively larger when obtained using organic acids compared to inorganic acids. NC-OA, NC-CA and NC-AA were formed within 100–300 nm, which were significantly larger than NC-SA, NC-HA and NC-PA (31–90 nm). The smallest NCCs were produced when using sulfuric acid with the average size was determined at 31 nm. Small particle size with narrow particle distribution indicated the high stability of NCCs in water suspension.

Zeta potential analysis determined the surface charge of material that can be used to evaluate the dispersion and the stability of nanocellulose suspension. Ideally, nanocrystalline cellulose should have high zeta potential to prevent agglomeration between the colloidal suspension, consequently increased the dispersion degree [53]. The zeta potential values of NCCs hydrolyzed with inorganic acid were determined at −37.9 ± 2.4 mV, −33.2 ± 0.3 mV and −28.9 ± 2.1 mV for NC-SA, NC-HA and NC-PA samples, respectively. Meanwhile, the zeta potential values for NC-OA, NC-CA and NC-AA samples were measured at −28.0 ± 1.9 mV, −28.3 ± 0.9 mV and −23.4 ± 0.6 mV respectively. The stability of colloidal suspension requires zeta potential value greater than -30 mV. Meanwhile agglomeration was prone to happen if the value was less than −15 mV [39,54]. The small zeta potential value (<−15 mV) also implied insufficient charges on the surface of NCCs resulting in a weak electrostatic repulsion ([55]; B. [56]).

Large NCC particles have a higher level of intrinsic hydroxyl group, caused the formation of a less stable nanocellulose suspension that insoluble in water [57]. Apart from that, the NCCs hydrolyzed using inorganic acid showed a higher negative charge value than the NCCs obtained from organic acid due to the strong adsorption of counter anion on the cellulose surface [58]. NCC prepared using sulfuric acid showed a higher colloidal stability due to the presence of sulfate groups on the NCC that enhanced the repulsive forces, resulted in the negative zeta potential value at −37.9 ± 2.4 mV [59]. NCC prepared using HCl and H_3PO_4 showed relatively weak negative charged compared to H_2SO_4 [58,60]. The presence of anionic mineral on the NCCs that were hydrolyzed using inorganic acid was confirmed by EDS (Fig. S1). NC-SA has a weak sulfur peak at 0.65% compared to the carbon peak at 32.63% (Table S1). The zeta potential value of NC-AA was determined at −23.4 ± 0.6 mV, significantly lower than the rest of NCCs.

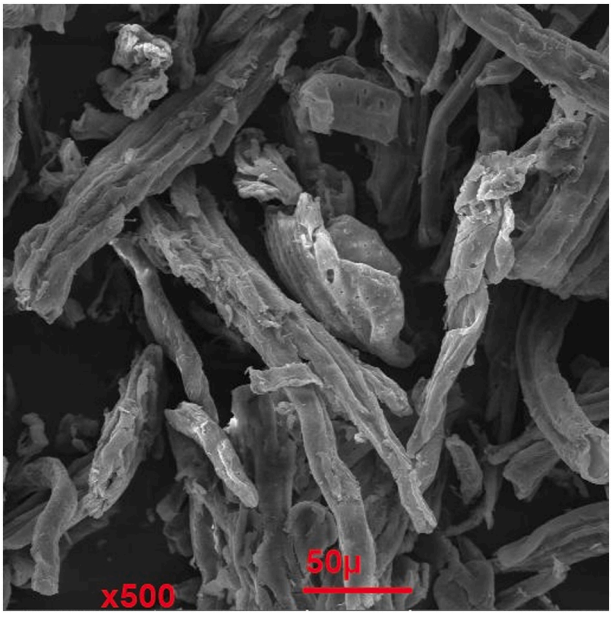

Fig. 5. SEM analysis of cellulose from pepper waste.

3.2.5. Morphological analysis

TEM analysis was used to analyze the morphology of NCCs powder obtained from hydrolysis using various types of inorganic acids and organic acids. Note that the cellulose used for hydrolysis showed the average diameter of 38.45 ± 2.2 µm with random fibrous structures (Fig. 5).

TEM analysis and the particle size distribution of NCCs isolated using inorganic acid in Fig. 6 showed all the NCCs produced from H_2SO_4, HCl and H_3PO_4 have spherical structures with diameter less than 100 nm. The average diameter of NC-SA, NC-HA and NC-PA were determined at 33.41 ± 14.7; 50.7 ± 11.6 and 67.8 ± 5.1 nm, respectively (Table 2). The spherical NCCs were interconnected to form a chain like network

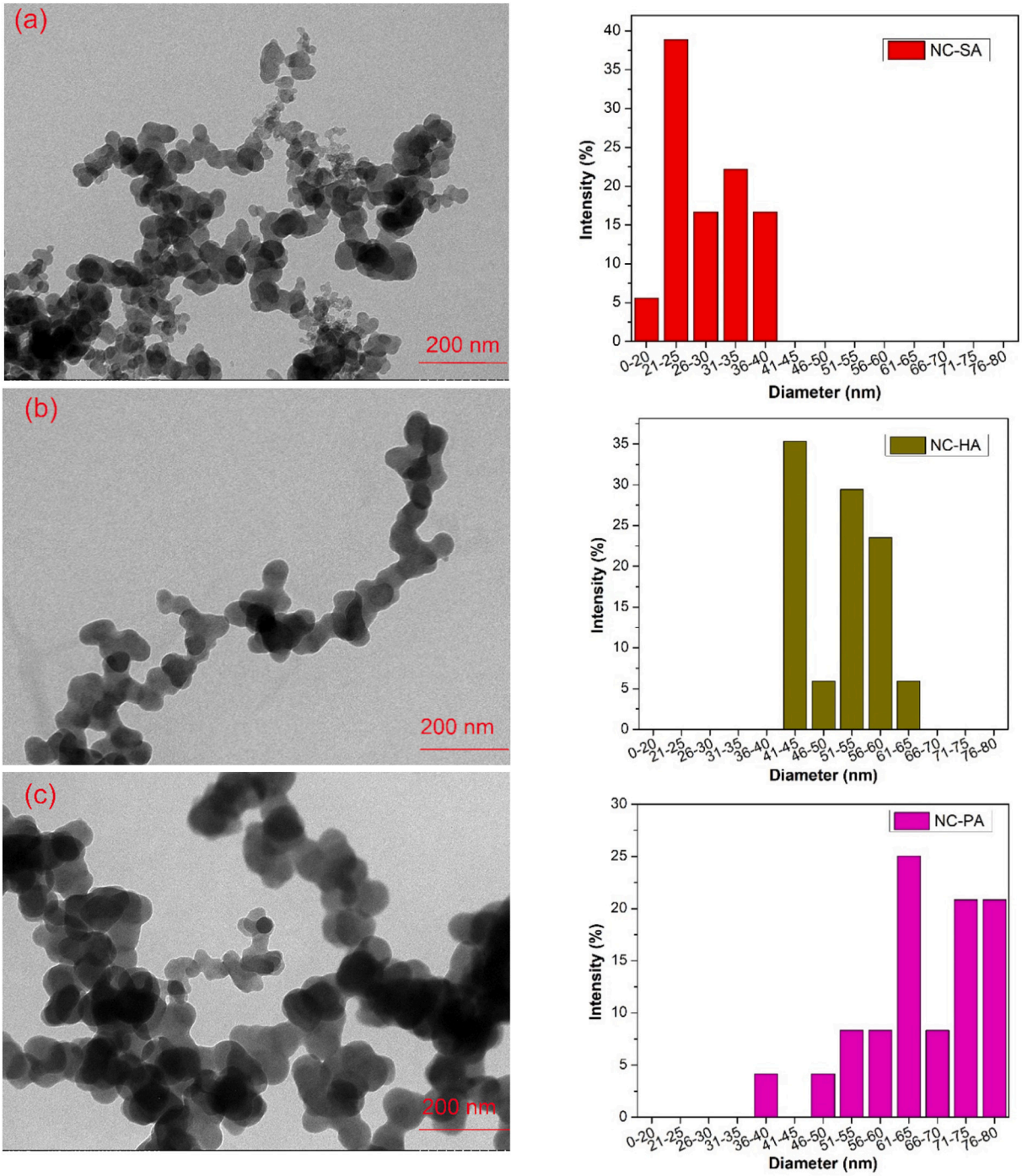

Fig. 6. TEM analysis and diameter distribution of NC-SA (a), NC-HA (b), and NC-PA (c).

presumably via interfacial hydrogen bonds formation [61]. When organic acids were used in hydrolysis, the NCCs showed the formation of rod-like shape structures (Fig. 7) with the average diameter were determined at 21.68; 23.22 and 48.73 nm for the respective NC-OA, NC-PA, and NC-AA. The lengths of the rods were determined at 210–321 nm.

3.2.6. *Thermal analysis*

TG-DTG analysis of PW, PW-C and NCCs obtained from hydrolysis using organic acids and inorganic acids were shown in Fig. 8. The initial temperature (T_{onset}) and the maximum temperature of thermal degradation (T_{peak}) were summarized in Table 3. PW sample showed three degradation stages at 100 °C, 241 °C and 313.7 °C. Initial degradation at temperature below 100 °C was due to the evacuation of physisorbed water. Generally, hemicellulose has a lower thermal stability than cellulose, and therefore the shoulder peak at 241 °C on PW was suggested due to the degradation of hemicellulose [62]. PW and PW-C showed T_{peak} value of 313.7 °C and 328.7 °C, respectively. All the NCCs derived from PW-C have a higher thermal stability than PW and PW-C. Meanwhile, the NCCs hydrolyzed from organic acids have relatively a higher stability at 346–351 °C than the NCCs from inorganic acids. The high thermal stability of NCC was ascribed to the presence of a highly crystalline cellulose as the results of removal of amorphous fragments and lignin residues within the cellulose structures [63] (Fig. 8).

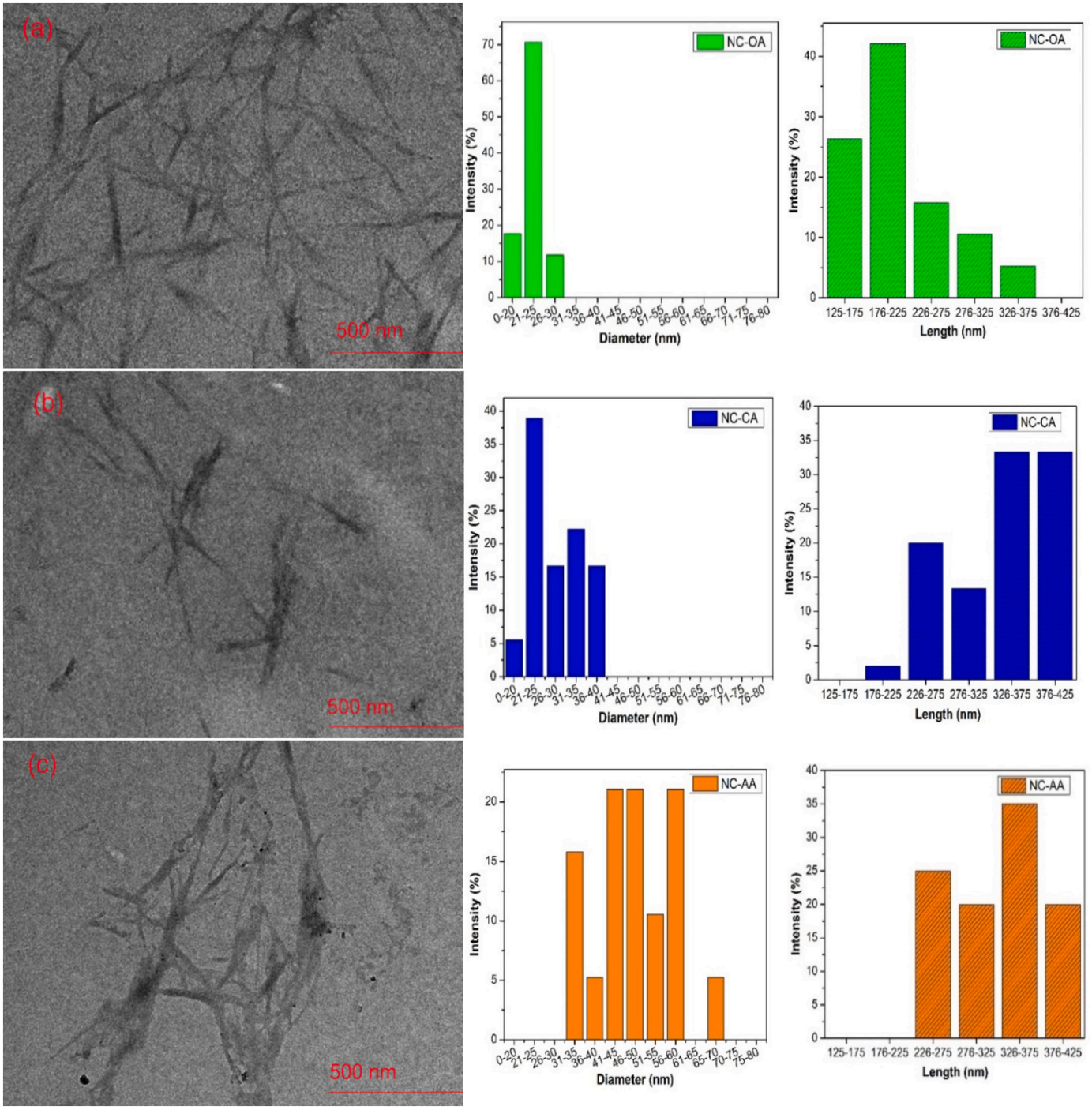

Fig. 7. TEM analysis and diameter distribution of NC-OA (a), NC-CA (b), NC-AA (c).

It is apparent that thermal stability of NCC is closely related to the particle size and the crystallinity. NCC obtained using inorganic acid showed the onset temperature at 298–300 °C compared to NCC hydrolyzed using organic acid. In general, small NCC particles have a higher surface area, and was suggested to contain a partial structural disorder [22]. Therefore, the decomposition required less thermal energy and occurred at lower temperatures (Jieng and Hsieh, 2013). Furthermore, thermal stability of NCC is influenced by the presence of the counter anions on the structure [58]. The presence of sulfate, chloride and phosphate groups on NCC as evidenced from EDX analysis (Supplementary document) reduced the initial degradation temperature by reducing the activation energy during pyrolysis. The anion is also suggested to act as catalysts in dehydration reaction [16,22,28,58,64]. The carbon residue of NC-SA sample was determined at 30.47% which was higher than the rest of NCCs.

3.2.7. The effect of inorganic acid and organic acid on the morphology of nanocellulose

Facile hydrolysis and sonication using organic acids and inorganic acids were able to control the morphology of NCCs isolated from pepper waste. TEM analysis provided evidence for organic acids ability to produce a rod-shaped NCC, meanwhile inorganic acids formed spherical-shaped NCC. Isolation of NCC using acid hydrolysis is a random process results in the formation of various structure and

Table 3
Thermal degradation temperature and weight loss at 600 °C of prepared nanocellulose products.

Sample	Thermal degradation temperature (°C)		Weight loss at 600 °C (%)
	Initial degradation	Max degradation	
PW	235.8	313.7	27.1
PW-C	269.1	328.7	22.4
NC-SA	300.6	345.6	30.5
NC-HA	291.5	343.7	17.2
NC-PA	298.3	333.2	16.2
NC-OA	311.2	346.5	9.9
NC-CA	310.1	349.0	12.6
NC-AA	308.2	351.2	11.4

morphology. Hydrolysis using sulfuric acid was reported to form cellulose nano whisker [25], ribbon-like nanocellulose [65], nanofiber cellulose [22] and spherical shape nanocellulose [26]. Meanwhile citric acid was reported to produce rod-shaped NCCs (Nagarajan, Balaji, Kasi Rajan, & Ramanujam, 2020) and cellulose nanofibrils [66]. However, the distinctive differences on the morphology of NCCs from cellulose pepper waste were observed in this study when inorganic acids and organic acids were used in hydrolysis. Fig. 9 summarized the isolation of nanocrystalline cellulose from pepper waste cellulose fiber. Inorganic acid is rapidly dissociated into H^+ to depolymerize cellulose molecules. Sonication accelerated the hydrolysis of cellulose by developing a continuous cavitation bubbles to release energy and mechanical shock wave that caused disruption of the hydrogen bond network [32,33,67,68].

Inorganic acid continuously released H^+ to further hydrolyze the depolymerized micro-cellulose into spherical nanoparticles. It is understood that acid hydrolysis of cellulose is a process involving the dissociation of hydrogen bonding between polymeric cellulose chain [52]. The dissociation of polymeric cellulose chain exposed the amorphous fragment for further dissolution into sugar molecules. Hydrolysis

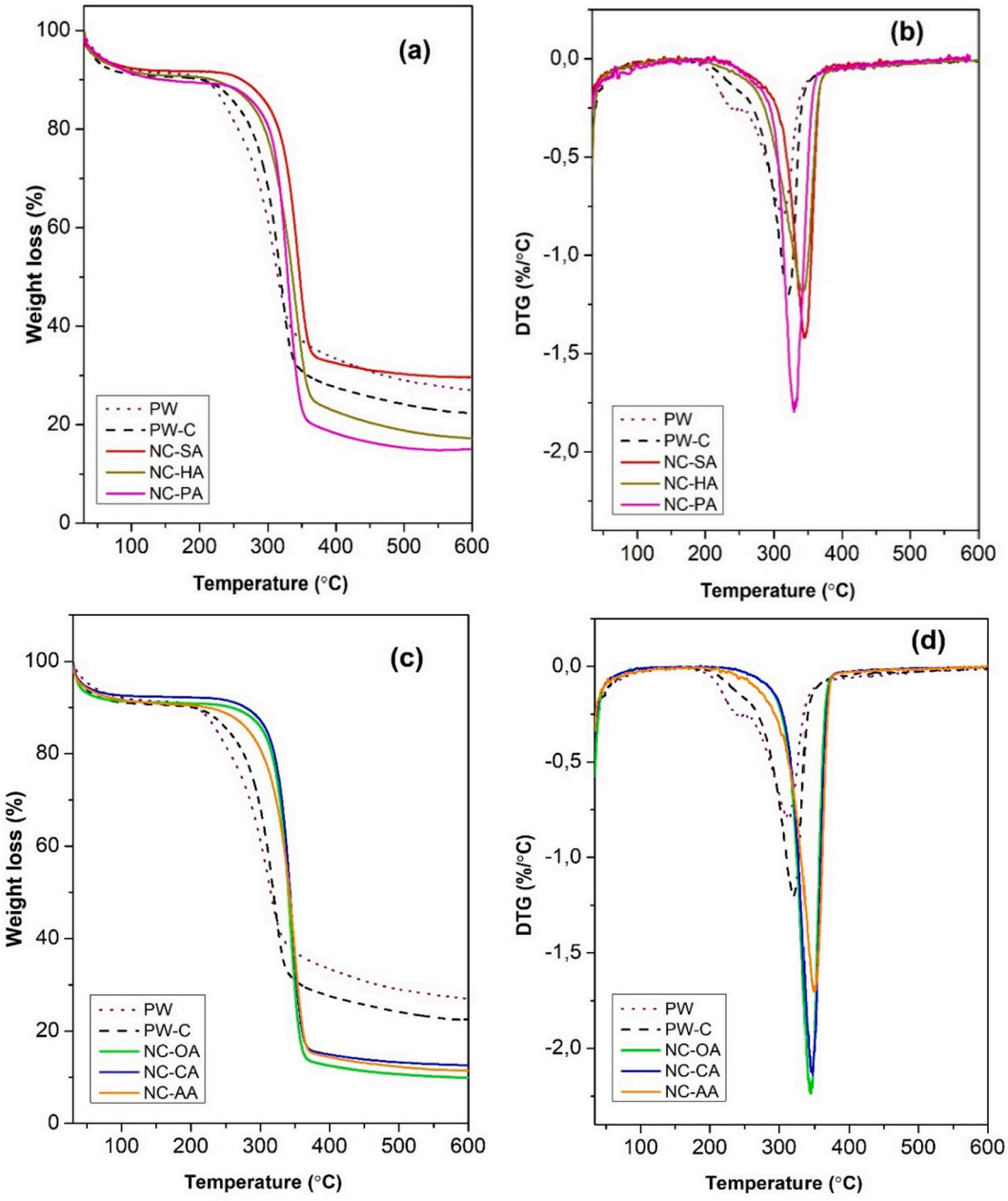

Fig. 8. TG-DTG curves of PW nanocellulose hydrolyzed by (a-b) inorganic acids and (c-d) organic acids.

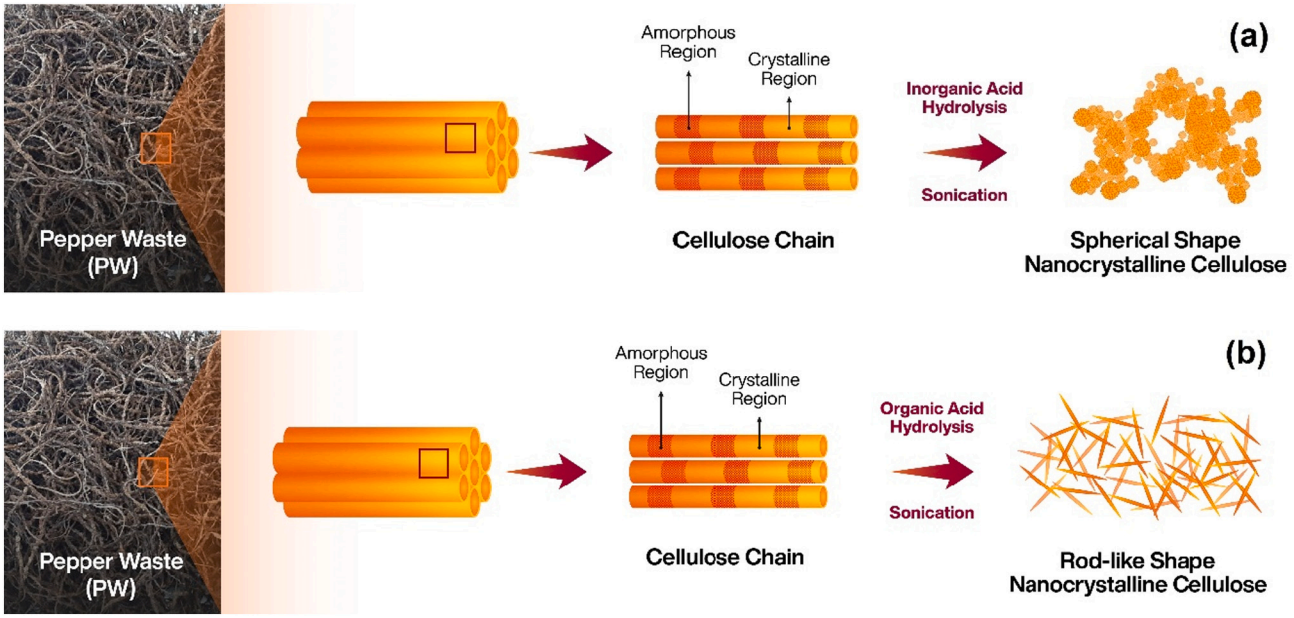

Fig. 9. Illustration of PW-C hydrolysis into spherical shape nanocellulose using inorganic acid (a) and hydrolysis into rod-like shape nanocellulose using organic acid (b).

of amorphous cellulose occurred faster than the crystalline cellulose thus at controlled hydrolysis time, high crystalline cellulose can be produced. The formation of smaller spherical NCC was proposed based on the ability of fully dissociated H^+ ion from inorganic acid to dissociate the β-1,4-glycosidic bonds, results in the formation of monocrystal cellulosic fragments. The presence of residual anion residues further stabilized the monocrystals from agglomeration by protecting the surface with the negative charge counter anion, which consequently created strong repulsive forces. On the other hand, the nature of organic acid dissociation which is restricted by equilibrium reduced the efficiency of hydrolysis process. Therefore, organic acid only removed the amorphous cellulose, results in the formation of highly crystalline NCCs. The lack of interaction between the weak counter anion of the organic acid with the cellulose reduced the repulsive forces, which allowed agglomeration to form a larger rod NCC structures.

4. Conclusion

This study reported a facile hydrolysis of lignocellulose pepper waste to form uniform rod-shaped and spherical-shaped NCCs by utilization of organic acids and inorganic acids. The hydrolysis was optimized by varying the duration of sonication times in order to obtain high NCCs yield and crystallinity. Nanocellulose with optimum crystallinity was produced at 15 min of sonication time regardless of the types of acids using in hydrolysis. The absence of hemicellulose and lignin in the resulting nanocellulose were confirmed by FTIR spectra, meanwhile the adsorption bands corresponded to cellulose structure were remained unchanged. The crystallinity and thermal stability of NCCs were higher than cellulose and pepper stalk waste (PW) indicating the enhancement of physical characteristic of NCCs. Hydrolysis using inorganic acids (HCl, H_2SO_4, H_3PO_4) formed spherical-shaped NCCs with a smaller diameter and a negatively charged surface. Hydrolysis using organic acids (acetic acid, oxalic acid and citric acid) produced rod-shaped NCCs with a relatively larger structure. The yield and the particles size were smaller for NCCs produced from inorganic acid, and the NCCs also exhibited low crystallinity, narrow particle distribution and high zeta potential when compared to NCCs obtained using organic acids. This study demonstrated the abundant pepper stalk waste can be converted into a value added nanocrystalline cellulose, in which the morphology and physicochemical properties can be controlled depending on the type of acid used in hydrolysis.

Declaration of competing interest

The authors declare that they have no known competing financial interests or personal relationships that could have appeared to influence the work reported in this paper.

Acknowledgement

The authors would like to acknowledge Kementerian Pendidikan Kebudayaan Riset dan Teknologi, Indonesia for the financial and technical support under Doctoral Research Grant (PDD) 860/PKS/ITS/2021 awarded to Holilah and Didik Prasetyoko.

Appendix A. Supplementary data

Supplementary data to this article can be found online at https://doi.org/10.1016/j.ijbiomac.2022.02.045.

References

[1] H. Holilah, D. Prasetyoko, R. Ediati, H. Bahruji, A.A. Jalil, A. Asranudin, S. D. Anggraini, Hydrothermal assisted isolation of microcrystalline cellulose from pepper (Piper nigrum L.) processing waste for making sustainable bio-composite, J. Clean. Prod. 305 (2021), 127229, https://doi.org/10.1016/J.JCLEPRO.2021.127229.
[2] A.H. Bhat, Y.K. Dasan, I. Khan, H. Soleimani, A. Usmani, Application of nanocrystalline cellulose: processing and biomedical applications, in: Cellulose-Reinforced Nanofibre Composites: Production, Properties and Applications, 2017, pp. 215–240, https://doi.org/10.1016/B978-0-08-100957-4.00009-7.
[3] M. Asghari, A.A.K. Zarchi, R.A. Taheri, Preparation and characterization nanocrystalline cellulose as a food additive to produce healthy biscuit cream, Starch - Stärke 73 (3–4) (2021), 2000033, https://doi.org/10.1002/STAR.202000033.
[4] C. Amara, A. El Mahdi, R. Medimagh, K. Khwaldia, Nanocellulose-based composites for packaging applications, Curr. Opin. Green Sustain. Chem. 31 (2021), 100512, https://doi.org/10.1016/J.COGSC.2021.100512.
[5] R.A. Ilyas, S.M. Sapuan, M.R. Ishak, Isolation and characterization of nanocrystalline cellulose from sugar palm fibres (Arenga pinnata), Carbohydr. Polym. 181 (2018) 1038–1051, https://doi.org/10.1016/j.carbpol.2017.11.045.
[6] E. Syafri, Jamaluddin, S. Wahono, A. Irwan, M. Asrofi, N.H. Sari, A. Fudholi, Characterization and properties of cellulose microfibers from water hyacinth filled sago starch biocomposites 137 (2019) 119–125, https://doi.org/10.1016/J.IJBIOMAC.2019.06.174.

[7] Rushdan Ahmad Ilyas, S.M. Sapuan, R. Ibrahim, H. Abral, M.R. Ishak, E. S. Zainudin, R. Jumaidin, Sugar palm (Arenga pinnata (Wurmb.) Merr) cellulosic fibre hierarchy: a comprehensive approach from macro to nano scale, J. Mater. Res. Technol. 8 (3) (2019) 2753–2766, https://doi.org/10.1016/J.JMRT.2019.04.011.

[8] A.K. Mohanty, M. Misra, G. Hinrichsen, Biofibres, biodegradable polymers and biocomposites: an overview 276–277 (2000, March 1) 1–24, https://doi.org/10.1002/(SICI)1439-2054(20000301)276:1<1::AID-MAME1>3.0.CO;2-W.

[9] A. Kumar, Y.S. Negi, V. Choudhary, N.K. Bhardwaj, Characterization of cellulose nanocrystals produced by acid-hydrolysis from sugarcane bagasse as agro-waste, J. Mater. Phys. Chem. 2 (1) (2014) 1–8, https://doi.org/10.12691/jmpc-2-1-1.

[10] C.A.D.C. Mendes, N.M.S. Ferreira, C.R.G. Furtado, A.M.F. De Sousa, Isolation and characterization of nanocrystalline cellulose from corn husk, Mater. Lett. 148 (2015) 26–29, https://doi.org/10.1016/j.matlet.2015.02.047.

[11] V.A. Barbash, O.V. Yaschenko, O.M. Shniruk, Preparation and properties of nanocellulose from organosolv straw pulp, Nanoscale Res. Lett. 12 (1) (2017) 1–8, https://doi.org/10.1186/s11671-017-2001-4.

[12] M. Mahardika, H. Abral, A. Kasim, S. Arief, M. Asrofi, Production of nanocellulose from pineapple leaf fibers via high-shear homogenization and ultrasonication, Fibers 6 (2) (2018) 1–12, https://doi.org/10.3390/fib6020028.

[13] M. Dominic, R. Joseph, P.M. Sabura Begum, B.P. Kanoth, J. Chandra, S. Thomas, Green tire technology: effect of rice husk derived nanocellulose (RHNC) in replacing carbon black (CB) in natural rubber (NR) compounding, Carbohydr. Polym. 230 (2020), 115620, https://doi.org/10.1016/j.carbpol.2019.115620.

[14] S. Rashid, H. Dutta, Characterization of nanocellulose extracted from short, medium and long grain rice husks, Ind. Crop. Prod. 154 (2020), 112627, https://doi.org/10.1016/j.indcrop.2020.112627.

[15] N. Sai Prasanna, J. Mitra, Isolation and characterization of cellulose nanocrystals from Cucumis sativus peels, Carbohydr. Polym. 247 (2020), 116706, https://doi.org/10.1016/j.carbpol.2020.116706.

[16] Z. Wang, Z. Yao, J. Zhou, M. He, Q. Jiang, S. Li, Y. Ma, M. Liu, S. Luo, Isolation and characterization of cellulose nanocrystals from pueraria root residue, Int. J. Biol. Macromol. 129 (2019) 1081–1089, https://doi.org/10.1016/j.ijbiomac.2018.07.055.

[17] A.P.M. Silva, A.V. Oliveira, S.M.A. Pontes, A.L.S. Pereira, M.de sá M. Souza Filho, M.F. Rosa, H.M.C. Azeredo, Mango kernel starch films as affected by starch nanocrystals and cellulose nanocrystals, Carbohydr. Polym. 211 (2019) 209–216, https://doi.org/10.1016/j.carbpol.2019.02.013.

[18] B.M. Cherian, L.A. Pothan, T. Nguyen-Chung, G. Mennig, M. Kottaisamy, S. Thomas, A novel method for the synthesis of cellulose nanofibril whiskers frombanana fibers and characterization, J. Agric. Food Chem. 56 (14) (2008) 5617–5627, https://doi.org/10.1021/jf8003674.

[19] B.M. Cherian, A.L. Leão, S.F. de Souza, S. Thomas, L.A. Pothan, M. Kottaisamy, Isolation of nanocellulose from pineapple leaf fibres by steam explosion, Carbohydr. Polym. 81 (3) (2010) 720–725, https://doi.org/10.1016/j.carbpol.2010.03.046.

[20] B.M. Cherian, L.A. Pothan, T. Nguyen-Chung, G. Mennig, M. Kottaisamy, S. Thomas, A novel method for the synthesis of cellulose nanofibril whiskers from banana fibers and characterization, J. Agric. Food Chem. 56 (14) (2008) 5617–5627, https://doi.org/10.1021/jf8003674.

[21] J. Henschen, D. Li, M. Ek, Preparation of cellulose nanomaterials via cellulose oxalates, Carbohydr. Polym. 213 (2019) 208–216, https://doi.org/10.1016/j.carbpol.2019.02.056.

[22] C. Liu, B. Li, H. Du, D. Lv, Y. Zhang, G. Yu, X. Mu, H. Peng, Properties of nanocellulose isolated from corncob residue using sulfuric acid, formic acid, oxidative and mechanical methods, Carbohydr. Polym. 151 (2016) 716–724, https://doi.org/10.1016/j.carbpol.2016.06.025.

[23] R. Poonguzhali, S. Khaleel Basha, V. Sugantha Kumari, Synthesis of alginate/nanocellulose bionanocomposite for in vitro delivery of ampicillin, Polym. Bull. 75 (9) (2018) 4165–4173, https://doi.org/10.1007/s00289-017-2253-2.

[24] Y. Ma, Q. Xia, Y. Liu, W. Chen, S. Liu, Q. Wang, Y. Liu, J. Li, H. Yu, Production of nanocellulose using hydrated deep eutectic solvent combined with ultrasonic treatment, ACS Omega 4 (2019) 8539–8547, https://doi.org/10.1021/acsomega.9b00519.

[25] M.F. Rosa, E.S. Medeiros, J.A. Malmonge, K.S. Gregorski, D.F. Wood, L.H. C. Mattoso, S.H. Imam, Cellulose nanowhiskers from coconut husk fibers: effect of preparation conditions on their thermal and morphological behavior, Carbohydr. Polym. 81 (1) (2010) 83–92, https://doi.org/10.1016/j.carbpol.2010.01.059.

[26] J. Zhang, T.J. Elder, Y. Pu, A.J. Ragauskas, Facile synthesis of spherical cellulose nanoparticles, Carbohydr. Polym. 69 (3) (2007) 607–611, https://doi.org/10.1016/j.carbpol.2007.01.019.

[27] L. Pachuau, R.S. Dutta, L. Hauzel, T.B. Devi, D. Deka, Evaluation of novel microcrystalline cellulose from Ensete glaucum (Roxb.) cheesman biomass as sustainable drug delivery biomaterial, Carbohydr. Polym. 206 (2019) 336–343, https://doi.org/10.1016/j.carbpol.2018.11.013.

[28] K.S. Prado, M.A.S. Spinacé, Isolation and characterization of cellulose nanocrystals from pineapple crown waste and their potential uses, Int. J. Biol. Macromol. 122 (2019) 410–416, https://doi.org/10.1016/j.ijbiomac.2018.10.187.

[29] T.L. Traynham, D.J. Myers, A.L. Carriquiry, L.A. Johnson, Evaluation of water-holding capacity for wheat-soy flour blends, J. Am. Oil Chem. Soc. 84 (2) (2007) 151, https://doi.org/10.1007/S11746-006-1018-0.

[30] O.A. Adetunji, M.A. Odeniyi, Material and compression properties of Cedrela odorata gum co-processed with plantain starch and microcrystalline cellulose, Polym Med. 46 (1) (2016) 35–43, https://doi.org/10.17219/PIM/64924.

[31] L. Segal, J.J. Creely, A.E. Martin, C.M. Conrad, An empirical method for estimating the degree of crystallinity of native cellulose using the X-ray diffractometer, Text. Res. J. 29 (10) (1959) 786–794, https://doi.org/10.1177/004051755902901003.

[32] S.B.A. Hamid, S.K. Zain, R. Das, G. Centi, Synergic effect of tungstophosphoric acid and sonication for rapid synthesis of crystalline nanocellulose, Carbohydr. Polym. 138 (2016) 349–355, https://doi.org/10.1016/j.carbpol.2015.10.023.

[33] S.B.A. Hamid, S.K. Zain, R. Das, G. Centi, Synergic effect of tungstophosphoric acid and sonication for rapid synthesis of crystalline nanocellulose, Carbohydr. Polym. 138 (2016) 349–355, https://doi.org/10.1016/j.carbpol.2015.10.023.

[34] X. Wang, G. Fang, C. Hu, T. Du, Application of ultrasonic waves in activation of microcrystalline cellulose, J. Appl. Polym. Sci. 109 (5) (2008) 2762–2767, 10.1002/app.

[35] H.Y. Kim, J.A. Han, D.K. Kweon, J.D. Park, S.T. Lim, Effect of ultrasonic treatments on nanoparticle preparation of acid-hydrolyzed waxy maize starch, Carbohydr. Polym. 93 (2) (2013) 582–588, https://doi.org/10.1016/j.carbpol.2012.12.050.

[36] W. Li, J. Yue, S. Liu, Preparation of nanocrystalline cellulose via ultrasound and its reinforcement capability for poly(vinyl alcohol) composites, Ultrason. Sonochem. 19 (3) (2012) 479–485, https://doi.org/10.1016/j.ultsonch.2011.11.007.

[37] K. Wahyuningsih, E.S. Iriani, F. Fahma, Utilization of cellulose from pineapple leaf fibers as nanofiller in polyvinyl alcohol-based film, Indones. J. Chem. 16 (2) (2016) 181–189, https://doi.org/10.14499/ijc-v16i2p181-189.

[38] A. Dufresne, Nanocellulose: a new ageless bionanomaterial, Mater. Today 16 (2013, June 1) 220–227, https://doi.org/10.1016/j.mattod.2013.06.004.

[39] J.P.S. Morais, M.D.F. Rosa, M.D.S.M. De Souza Filho, L.D. Nascimento, D.M. Do Nascimento, A.R. Cassales, Extraction and characterization of nanocellulose structures from raw cotton linter, Carbohydr. Polym. 91 (1) (2013) 229–235, https://doi.org/10.1016/j.carbpol.2012.08.010.

[40] K.J. Nagarajan, A.N. Balaji, S.T. Kasi Rajan, N.R. Ramanujam, Preparation of bio-eco based cellulose nanomaterials from used disposal paper cups through citric acid hydrolysis, Carbohydr. Polym. 235 (2020), https://doi.org/10.1016/j.carbpol.2020.115997.

[41] S. Abdul Razak, A.H. Mahadi, R. Abdullah, H.M. Yasin, F. Ja'afar, N. Abdul Rahman, H. Bahruji, Biohydrogen production from photodecomposition of various cellulosic biomass wastes using metal-TiO2 catalysts, Biomass Convers. Biorefinery (2020) 1–12, https://doi.org/10.1007/s13399-020-01164-4.

[42] M. El Achaby, M. Ruesgas-Ramón, N.E.H. Fayoud, M.C. Figueroa-Espinoza, V. Trabadelo, K. Draoui, H. Ben Youcef, Bio-sourced porous cellulose microfibrils from coffee pulp for wastewater treatment, Cellulose 26 (6) (2019) 3873–3889, https://doi.org/10.1007/s10570-019-02344-w.

[43] T. Ganapathy, R. Sathiskumar, P. Senthamaraikannan, S.S. Saravanakumar, A. Khan, Characterization of raw and alkali treated new natural cellulosic fibres extracted from the aerial roots of banyan tree, Int. J. Biol. Macromol. 138 (2019) 573–581, https://doi.org/10.1016/J.IJBIOMAC.2019.07.136.

[44] C.S. Julie Chandra, P.K. Bipinbal, K.N. Sunil, Viscoelastic behaviour of silica filled natural rubber composites – correlation of shear with elongational testing, Polym. Test. 60 (2017) 187–197, https://doi.org/10.1016/j.polymertesting.2017.03.023.

[45] H.K. Singh, T. Patil, S.K. Vineeth, S. Das, A. Pramanik, S.T. Mhaske, Isolation of microcrystalline cellulose from corn stover with emphasis on its constituents: corn cover and corn cob, Mater. Today Proc. (2019), https://doi.org/10.1016/j.matpr.2019.12.065.

[46] S. Indran, R.E. Raj, Characterization of new natural cellulosic fiber from Cissus quadrangularis stem, Carbohydr. Polym. 117 (2015) 392–399, https://doi.org/10.1016/J.CARBPOL.2014.09.072.

[47] D. Trache, M.H. Hussin, C.T. Hui Chuin, S. Sabar, M.R.N. Fazita, O.F.A. Taiwo, T. M. Hassan, M.K.M. Haafiz, Microcrystalline cellulose: isolation, characterization and bio-composites application—a review 93 (2016, December 1) 789–804, https://doi.org/10.1016/j.ijbiomac.2016.09.056.

[48] R.D. Kalita, Y. Nath, M.E. Ochubiojo, A.K. Buragohain, Extraction and characterization of microcrystalline cellulose from fodder grass; Setaria glauca (L) P. Beauv, and its potential as a drug delivery vehicle for isoniazid, a first line antituberculosis drug, Colloids Surf. B: Biointerfaces 108 (2013) 85–89, https://doi.org/10.1016/j.colsurfb.2013.02.016.

[49] K.C.C.de C. Benini, H.J.C. Voorwald, M.O.H. Cioffi, M.C. Rezende, V. Arantes, Preparation of nanocellulose from Imperata brasiliensis grass using Taguchi method, Carbohydr. Polym. 192 (2018) 337–346, https://doi.org/10.1016/j.carbpol.2018.03.055.

[50] G. Kumar Rai, V.P. Singh, Study of fabrication and analysis of nanocellulose reinforced polymer matrix composites, Mater. Today Proc. (2020), https://doi.org/10.1016/j.matpr.2020.06.018.

[51] S. Mateo, S. Peinado, F. Morillas-Gutiérrez, M.D.La Rubia, A.J. Moya, Nanocellulose from agricultural wastes: products and applications—a review, Processes 9 (9) (2021) 1594, https://doi.org/10.3390/PR9091594, 2021, Vol. 9, Page 1594.

[52] Y.B. Huang, Y. Fu, Hydrolysis of cellulose to glucose by solid acid catalysts, Green Chem. 15 (5) (2013) 1095–1111, https://doi.org/10.1039/c3gc40136g.

[53] S. Naduparambath, J. T.V., V. Shaniba, S. M.P., A.K. Balan, E. Purushothaman, Isolation and characterisation of cellulose nanocrystals from sago seed shells, Carbohydr. Polym. 180 (April 2017) (2018) 13–20, https://doi.org/10.1016/j.carbpol.2017.09.088.

[54] M.S. Mohaiyiddin, O.H. Lin, W.T. Owi, C.H. Chan, C.H. Chia, S. Zakaria, A. L. Villagracia, H.M. Akil, Characterization of nanocellulose recovery from Elaeis guineensis frond for sustainable development, Clean Techn. Environ. Policy 18 (8) (2016) 2503–2512, https://doi.org/10.1007/s10098-016-1191-2.

[55] A.C. Corrêa, E.M. de Teixeira, L.A. Pessan, L.H.C. Mattoso, Cellulose nanofibers from curaua fibers, Cellulose 17 (6) (2010) 1183–1192, https://doi.org/10.1007/s10570-010-9453-3.

[56] B. Li, W. Xu, D. Kronlund, A. Määttänen, J. Liu, J.H. Smått, J. Peltonen, S. Willför, X. Mu, C. Xu, Cellulose nanocrystals prepared via formic acid hydrolysis followed

by TEMPO-mediated oxidation, Carbohydr. Polym. 133 (2015) 605–612, https://doi.org/10.1016/j.carbpol.2015.07.033.
[57] K. Rahbar Shamskar, H. Heidari, A. Rashidi, Study on nanocellulose properties processed using different methods and their aerogels, J. Polym. Environ. 27 (7) (2019) 1418–1428, https://doi.org/10.1007/s10924-019-01438-7.
[58] D. Klemm, F. Kramer, S. Moritz, T. Lindström, M. Ankerfors, D. Gray, A. Dorris, Nanocelluloses: a new family of nature-based materials, Angew. Chem. Int. Ed. 50 (24) (2011) 5438–5466, https://doi.org/10.1002/ANIE.201001273.
[59] R.H.F. Faradilla, G. Lee, A. Rawal, T. Hutomo, M.H. Stenzel, J. Arcot, Nanocellulose characteristics from the inner and outer layer of banana pseudo-stem prepared by TEMPO-mediated oxidation, Cellulose 23 (5) (2016) 3023–3037, https://doi.org/10.1007/s10570-016-1025-8.
[60] P. Lu, Y.Lo. Hsieh, Preparation and properties of cellulose nanocrystals: rods, spheres, and network, Carbohydr. Polym. 82 (2) (2010) 329–336, https://doi.org/10.1016/j.carbpol.2010.04.073.
[61] O. Van Den Berg, M. Schroeter, J.R. Capadona, C. Weder, Nanocomposites based on cellulose whiskers and (semi)conducting conjugated polymers, J. Mater. Chem. 17 (26) (2007) 2746–2753, https://doi.org/10.1039/b700878c.
[62] C.J. Chirayil, J. Joy, L. Mathew, M. Mozetic, J. Koetz, S. Thomas, Isolation and characterization of cellulose nanofibrils from Helicteres isora plant, Ind. Crop. Prod. 59 (2014) 27–34, https://doi.org/10.1016/j.indcrop.2014.04.020.
[63] Y. Qing, R. Sabo, J.Y. Zhu, U. Agarwal, Z. Cai, Y. Wu, A comparative study of cellulose nanofibrils disintegrated via multiple processing approaches, Carbohydr. Polym. 97 (1) (2013) 226–234, https://doi.org/10.1016/j.carbpol.2013.04.086.
[64] M. Roman, W.T. Winter, Effect of Sulfate Groups From Sulfuric Acid Hydrolysis on the Thermal Degradation Behavior of Bacterial Cellulose, 2004, https://doi.org/10.1021/BM034519+.
[65] B.S.L. Brito, F.V. Pereira, J.L. Putaux, B. Jean, Preparation, morphology and structure of cellulose nanocrystals from bamboo fibers, Cellulose 19 (5) (2012) 1527–1536, https://doi.org/10.1007/s10570-012-9738-9.
[66] T.J. Bondancia, J. De Aguiar, G. Batista, A.J.G. Cruz, J.M. Marconcini, L.H. C. Mattoso, C.S. Farinas, Production of nanocellulose using citric acid in a biorefinery concept: effect of the hydrolysis reaction time and techno-economic analysis, Ind. Eng. Chem. Res. 59 (25) (2020) 11505–11516, https://doi.org/10.1021/ACS.IECR.0C01359/SUPPL_FILE/IE0C01359_SI_002.XLSX.
[67] J. Guo, X. Guo, S. Wang, Y. Yin, Effects of ultrasonic treatment during acid hydrolysis on the yield, particle size and structure of cellulose nanocrystals, Carbohydr. Polym. 135 (2016) 248–255, https://doi.org/10.1016/j.carbpol.2015.08.068.
[68] N.A. Mohd Ishak, I. Khalil, F.Z. Abdullah, N. Muhd Julkapli, A correlation on ultrasonication with nanocrystalline cellulose characteristics, Carbohydr. Polym. 246 (2020), 116553, https://doi.org/10.1016/j.carbpol.2020.116553.